ACS APPLIED ENERGY MATERIALS

www.acsaem.org Article

Rational Design of Ultrastable Conjugated Microporous Polymers Based on Pyrene and Perylene Units as High-Performance Organic Electrode Materials for Supercapacitor Applications

Poonam Nagendra Singh, Mohamed Gamal Mohamed,* Swetha V. Chaganti, Santosh U. Sharma, Moshin Ejaz, Jyh-Tsung Lee, and Shiao-Wei Kuo*

Cite This: *ACS Appl. Energy Mater.* 2023, 6, 8277−8287 Read Online

ACCESS | Metrics & More | Article Recommendations | Supporting Information

ABSTRACT: We successfully synthesized three perylene dianhydride (PDI)-based conjugated microporous polymers (CMPs), namely, Py-Ph-Pery, TPE-Ph-Pery, and TPA-Ph-Pery CMPs, through a Suzuki−Miyaura coupling reaction. The precursors used in the reaction contained brominated compounds of pyrene (Py), tetraphenylethylene (TPE), triphenylamine (TPA), and 1,4-benzeneboronic acid, which were coupled with redox-active PDI unit. To evaluate the thermal stability, molecular structure, and porosity properties of the synthesized CMPs, we conducted an examination of their Brunauer−Emmett−Teller isotherm, along with spectroscopic and microscopic analyses. These CMPs demonstrated moderate thermal stability based on thermogravimetric analysis. In terms of electrochemical performance, the Py-Ph-Pery CMP exhibited a high capacitance of 300 F g^{-1} (measured at 0.5 A g^{-1}), indicating its excellent capacitive properties. Furthermore, the Py-Ph-Pery CMP displayed exceptional cycle stability at 10 A g^{-1}, retaining more than 93% of its capacity over 5000 cycles. The findings illustrate the potential of these CMPs for reliable and durable energy storage applications. Additionally, we utilized synthesized CMPs to assess the electrochemical characteristics of a symmetric coin supercapacitor. The results further validate the suitability of these CMPs for practical electrical energy storage applications, highlighting their significant promise.

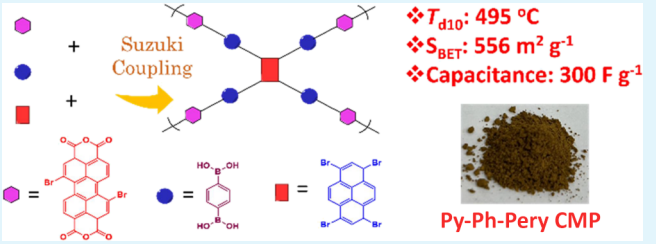

KEYWORDS: *perylene-3,4,9,10-tetracarboxylic acid dianhydride, Suzuki−Miyaura reaction, conjugated microporous polymers, porosity, supercapacitors*

INTRODUCTION

The escalating energy consumption has resulted in the exacerbation of global warming,[1−6] primarily caused by greenhouse gas emissions from the combustion of fossil fuels.[7,8] To tackle these challenges, it is crucial to prioritize the development of efficient energy storage technologies. In an ideal scenario, we should prioritize using healthier and more sustainable resources to meet the growing energy demand. Energy storage plays a vital role in realizing the full potential of green and renewable energy sources such as solar, wind, and biomass.[2,9−11] Among the various energy storage technologies available, rechargeable electrochemical energy storage stands out as a promising option due to its high efficiency, especially for larger smart-grid energy storage systems (ESSs).[12,13]

Batteries and supercapacitors (SCs) are two commonly used electrical energy storage technologies. SCs have drawn much interest because of their outstanding benefits against batteries and fuel cells. They exhibit remarkable rate performance, offering high power densities and extended cycling lives that often exceed 100,000 cycles. SCs use two in close proximity layers of opposing charge to serve as energy storage devices. They find applications in various electronic devices, memory backup systems, and electric vehicles.[14] SCs can be divided into two categories: electric double-layer capacitors (EDLCs) and pseudo-capacitors, based on different charge storage processes.[7,15−20] Among these, EDLCs, known for their exceptionally long cycle lifetimes, high power densities, low maintenance costs, and environmentally friendly compositions, are widely used as energy storage devices.[3,21−23] Overall, SCs, particularly EDLCs, are highly favored energy storage solutions due to their remarkable characteristics and wide range of applications. In the field of SCs, the commonly used electrode materials include metal oxides and hydroxides, porous carbon materials, and conductive polymers.[7] Among these, microporous materials have demonstrated a significant value in various academic and industrial applications.[24]

Received: June 6, 2023
Accepted: July 11, 2023
Published: July 24, 2023

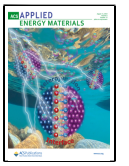

https://doi.org/10.1021/acsaem.3c01391
ACS Appl. Energy Mater. 2023, 6, 8277−8287

Conjugated microporous polymer (CMP) networks are gaining increasing importance in energy storage, catalysis, gas storage, and other areas.[25−31] CMPs are a type of organic porous polymers characterized by a conjugated framework and a structure featuring micropores.[32−36] These polymers have shown exceptional electrochemical performance in SC studies.[37] CMPs are a subclass of porous organic polymers that exhibit π-conjugation within their microporous structures.[38−40] The unique feature of CMPs lies in their ability to be synthesized with a wide range of architectures and characteristics, thanks to the availability of diverse building blocks and reaction pathways. The versatility and adjustability of CMPs make them highly desirable for SC applications. They offer the potential for developing efficient and customized electrode materials specifically tailored for ESSs.

Various methods have been employed to synthesize CMPs, including conventional coupling techniques like Sonogashira−Hagihara,[41−43] Suzuki−Miyaura,[44−47] and Yamamoto coupling,[47,48] as well as oxidative polymerization.[49−51] These methods have been used to create CMPs with diverse structures and properties.[52,53] In particular, quinones (phenols) and their derivatives, which are organic compounds with a benzoquinone structure, have been widely used in batteries and other devices that store energy.[54−56] With their outstanding cheap cost, morphological variety, great theoretical capacity, versatility, and sustainability, these molecules are a rare find. The favorable electrochemical characteristics of organic molecules, such as cycle stabilities and acceptable energy densities, have led to increased interest in their application within the field of SCs.[57,58] Recently, there has been growing attention toward the utilization of redox-active small organic compounds in organic SCs (OSCs).[56,59,60] OSCs possess the necessary redox properties, structural flexibility, sustainability, and a minimal ecological footprint. The potential of OSCs to offer effective and environmentally friendly energy storage solutions, combining the advantages of organic molecules with the desired characteristics of SCs, is what drives their increasing popularity.[59,60] Today, electrode materials derived from abundant natural sources are widely used. Small organic molecules intended for use as redox electrode materials in SCs must fulfill several requirements: (i) exhibit faradaic charge−discharge characteristics in the solid state within an aqueous electrolyte environment; (ii) be insoluble in the electrolyte during electrochemical processes; (iii) demonstrate cycling stability; and (iv) possess high power and energy densities.[59,60]

One class of compounds that have found application as electrodes in various SC systems is perylene dianhydride (PDI).[56,61] PDI offers key features, such as the creation of large surface area structures driven by interactions and the participation of delocalized electrons in reversible redox processes.[62] Pyrene (Py) has a distinctive planar fused ring structure and is made up of four benzene rings. Given its intriguing mix of electrical and structural features, Py, the smallest condensed polycyclic aromatic hydrocarbon, has received a great deal of research attention.[63,64] Py is utilized to enhance the charge transport properties of organic semiconductors based on *p*-conjugated systems by controlling molecule accumulation.[63,64] Py has a number of outstanding features, including heat stability, high fluorescence quantum efficiency, and high carrier mobility.[63,64] In this study, three PDI-based conjugated microporous polymers (Py-Ph-Pery, TPE-Ph-Pery, and TPA-Ph-Pery CMPs) were synthesized with high yields. To achieve this, a Suzuki−Miyaura coupling reaction was employed, combining different brominated derivatives of Py, TPE, and TPA moieties with Pery-Br_2 and $PhB(OH)_2$. The resulting three Pery-CMPs were thoroughly examined and analyzed to determine their molecular composition, thermal stability, porosity, surface morphologies, and crystallinity. The findings of these investigations were subsequently identified and discussed.

EXPERIMENTAL SECTION

Materials. 1,4-Benzeneboronic acid [$PhB(OH)_2$, 95%], Py (98%), N-bromosuccinimide (NBS, 99%), triphenylamine (TPA, 98%), potassium carbonate (K_2CO_3, 99.9%), bromine solution (Br_2), perylene-3,4,9,10-tetracarboxylic acid dianhydride (Pery, 97%) and anhydrous magnesium sulfate ($MgSO_4$, 99.5%) were purchased from Alfa Aesar. The details of the synthesis of the tetraphenyethene (TPE) monomer are given in our previous work.[3]

Synthesis of 1,1,2,2-Tetrakis(4-bromophenyl) Ethene (TPE-Br_4). In a 250 mL round-bottom flask, a solution was prepared by combining Br_2 (7.23 mL, 144.6 mmol) and TPE (6.0 g, 18.1 mmol).[3] To this mixture, glacial acetic acid (18 mL) and DCM (36 mL) were added. The solution was then cooled down to 0 °C for half an hour, followed by stirring at room temperature for 2 days to allow the reaction to proceed. After the reaction was complete, 100 mL of ice water was prepared. The reaction mixture was poured into the ice water and extracted using DCM. The resulting solution was treated with $MgSO_4$ to remove any remaining water. The solution was then subjected to rotary evaporation to remove $MgSO_4$, and methanol was added. The mixture was filtered to obtain a white powder as the final product [Scheme S1]. M.p.: 262 °C. FTIR: 3051 and 1572 (C═C). ^{1}H NMR: 7.3 (8H), 6.8 (8H). ^{13}C NMR: 142.3−122.8.

Synthesis of 1,3,6,8-Tetrabromopyrene (Py-Br_4). Py (2.0 g, 9.6 mmol) was added to a 500 mL round-bottom flask containing nitrobenzene (80 mL).[20] The mixture was continuously stirred using a magnetic stirrer for 4 h at a temperature of 120 °C. The solution was allowed to cool once the reaction was finished. After filtered out, ethanol was used to clean out the leftover solid. The resulting product exhibited a pale-yellow color [Scheme S2]. FTIR (cm^{-1}): 3054 (C−H stretching for the Py unit).

Synthesis of Tris(4-bromophenyl)amine (TPA-Br_3). TPA (1.63 mmol) was placed.[18] To this flask, NBS (4.8 g, 4.92 mmol) was added, which was previously dissolved in DMF (24 mL) in a dropwise manner. The reaction mixture was kept in an ice bath with magnetic stirring overnight. After the reaction was complete, the resulting mixture was rinsed with DCM and thoroughly washed. This process was performed to remove impurities and any unreacted compounds. Finally, a white powder was obtained as the product of the reaction [Scheme S3]. M.p.:142 °C (DSC). FTIR (cm^{-1}): 3078, 1618 (C═C). ^{1}H NMR: 6.94 (6H), 7.4 (d, 6H). ^{13}C NMR: 146.8−116.4.

Synthesis of 1,7-Dibromo Perylene Dianhydride (Pery-Br_2). In a round-bottom flask, Pery (2 g, 5.08 mmol) was dissolved in sulfuric acid (60 mL) while stirring at room temperature for 1 h. Following that, iodine (0.11 g, 0.4 mmol) was added, and the mixture was refluxed at 100 °C for 45 min. Afterward, a solution of bromine (4.88 g, 31 mmol) was added to the reaction mixture and left to react overnight at 100 °C. Once cooled down, water was added drop by drop to the mixture, resulting in the formation of a red precipitate. The precipitate was washed by H_2O and MeOH and subsequently dried, resulting in a yield of red-colored product [Scheme S4]. FTIR (Figure S1): 3064, 1781 (C═O).

Synthesis of Py-Ph-Pery, TPE-Ph-Pery, and TPA-Ph-Pery CMPs. Py-Br_4 (0.39 mmol), Pery-Br_2 (0.19 mmol), K_2CO_3 (3.11 mmol), $PhB(OH)_2$ (0.78 mmol), and $Pd(PPh_3)_4$ (0.04 mmol) were prepared in DMF and water. The mixture was then heated at 110 °C for 24 h. After the reaction, the resulting insoluble solid was separated by filtration. The solid product was then dried under vacuum at 90 °C for 24 h, resulting in the formation of Py-Ph-Pery CMP as a dark-brown solid. TPE-Ph-Pery CMP: TPE-Br_4 (0.32 mmol), Pery-Br_2 (0.16 mmol), $PhB(OH)_2$ (0.18 mmol), K_2CO_3 (2.53 mmol), and $Pd(PPh_3)_4$ (0.04 mmol) in DMF/H_2O to afford brown powder. TPA-Ph-Pery

https://doi.org/10.1021/acsaem.3c01391
ACS Appl. Energy Mater. 2023, 6, 8277−8287

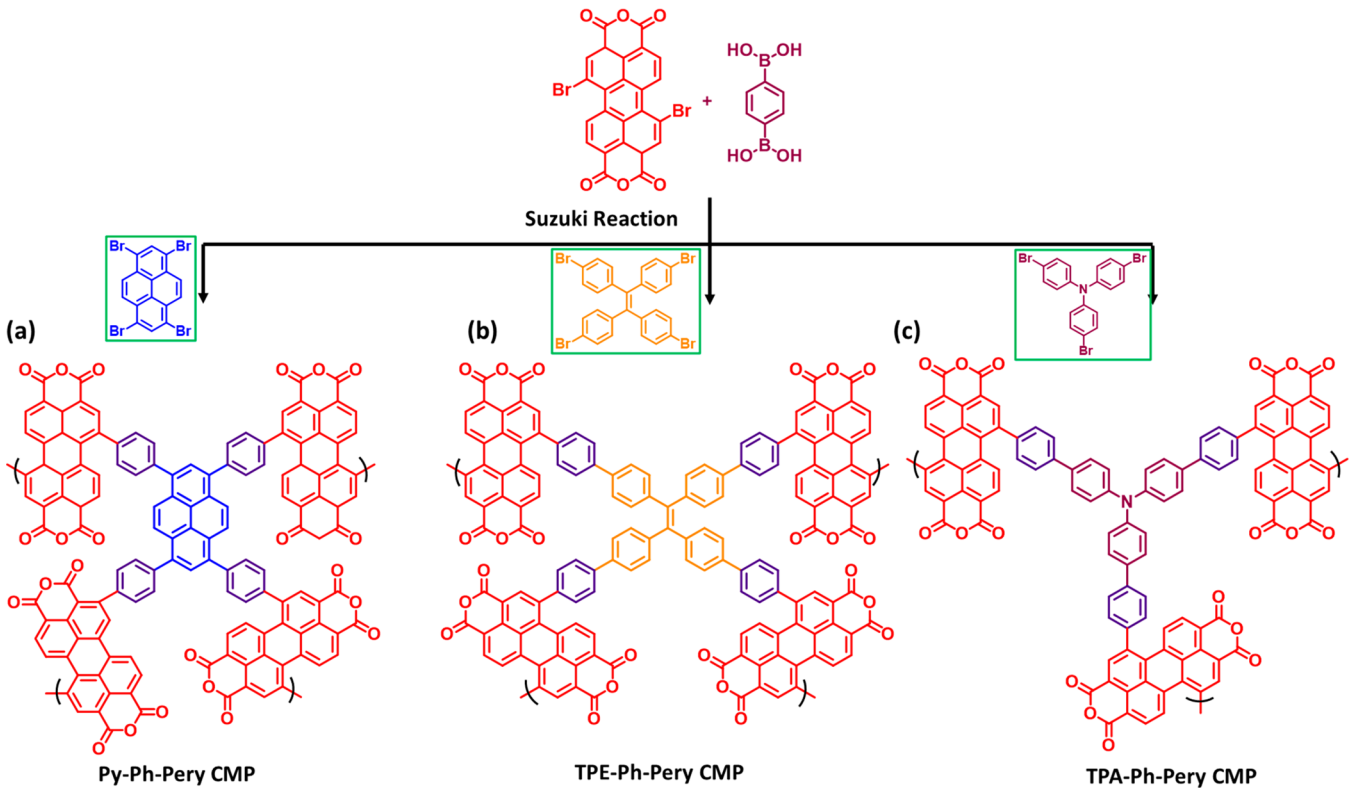

Figure 1. Preparation of the (a) Py-Ph-Pery, (b) TPE-Ph-Pery, and (c) TPA-Ph-Pery CMPs.

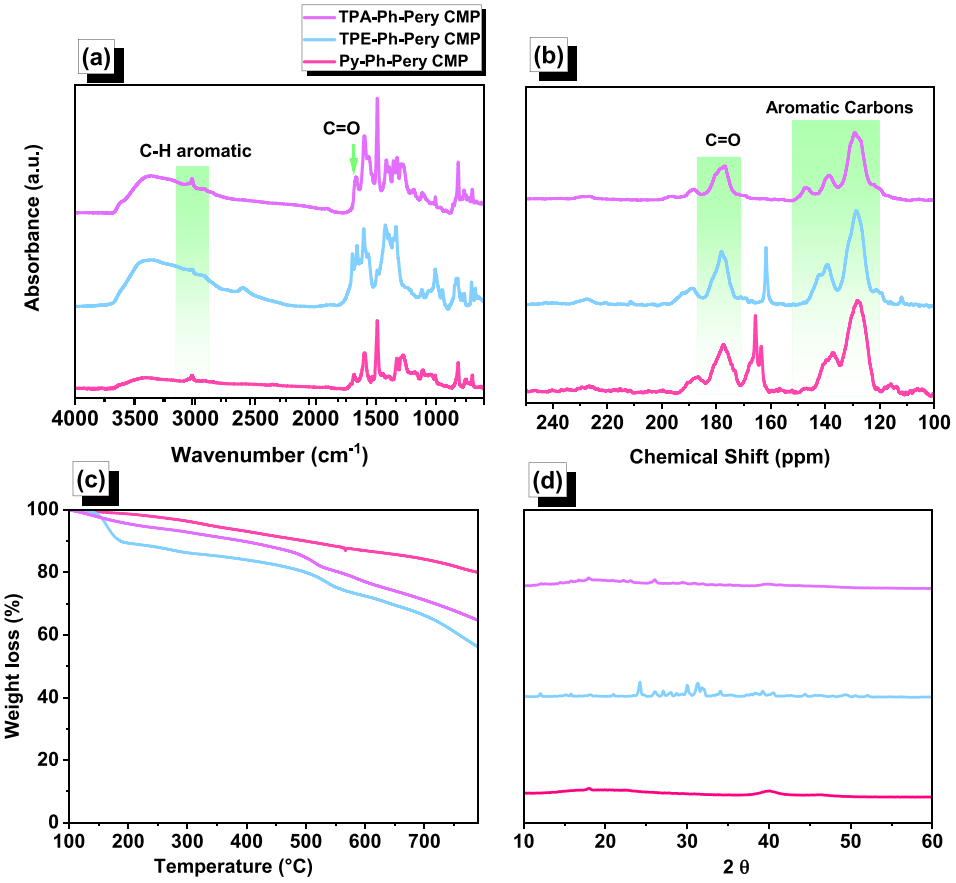

Figure 2. FTIR (a), ^{13}C NMR (b), TGA (c), and XRD (d) profiles of Py-Ph-Pery, TPE-Ph-Pery, and TPA-Ph-Pery CMPs.

https://doi.org/10.1021/acsaem.3c01391
ACS Appl. Energy Mater. 2023, 6, 8277−8287

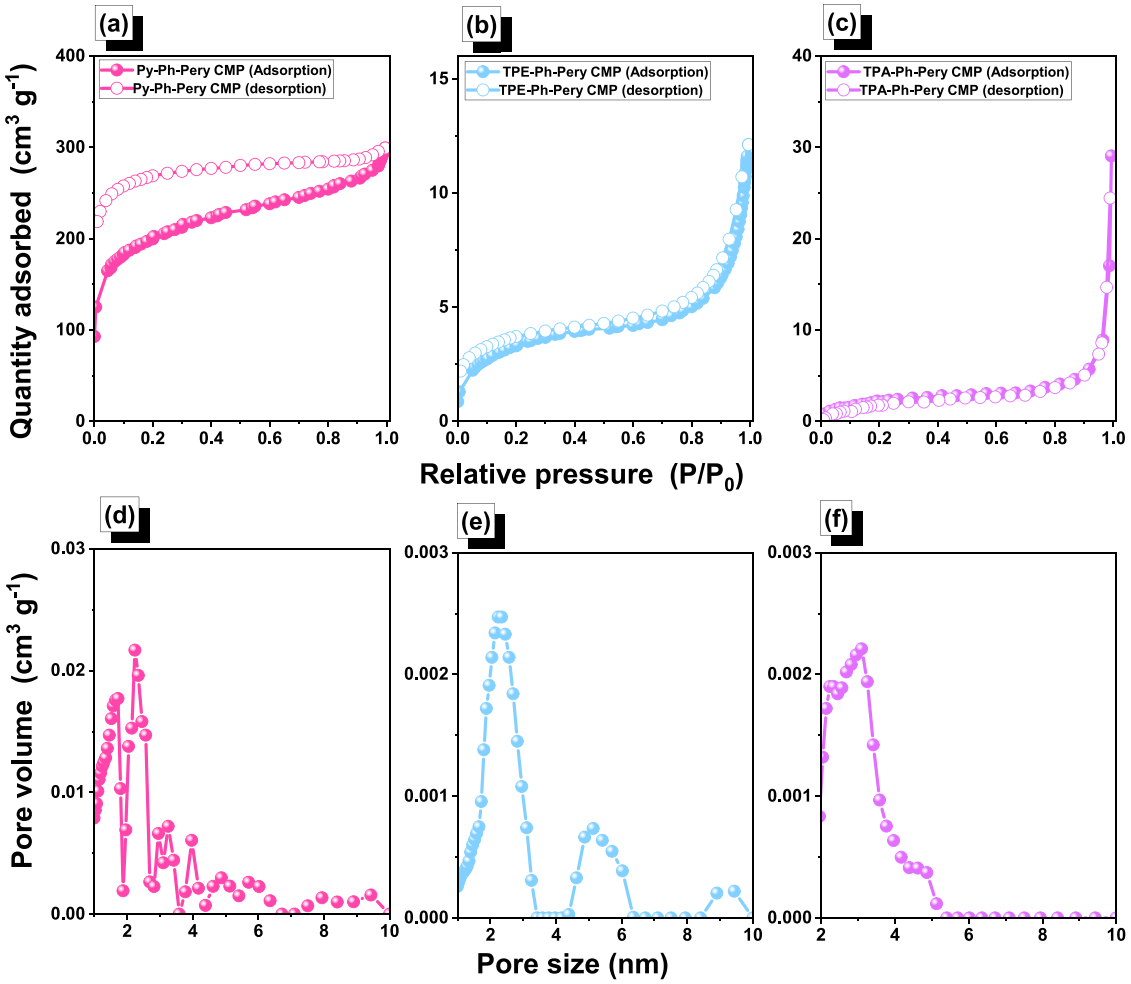

Figure 3. BET and pore diameter distribution profiles of Py-Ph-Pery (a, d), TPE-Ph-Pery (b, e), and TPA-Ph-Pery CMPs (c, f).

CMP: TPA-Br_3 (0.41 mmol), Pery-Br_2 (0.21 mmol), $PhB(OH)_2$ (0.66 mmol), K_2CO_3 (2.53 mmol), and $Pd(PPh_3)_4$ (0.04 mmol) to get a brown solid.

RESULTS AND DISCUSSION

We utilized the bromination reaction outlined in Schemes S1–S3 to prepare the brominated precursors of Py, TPE, and TPA. To generate the building unit Pery-Br_2, we reacted Pery with a solution of Br_2 in the presence of H_2SO_4 and traces of I_2 at 100 °C, as depicted in Scheme S4. Figure 1 showcases the synthetic methods employed to produce three Pery-CMPs: Py-Ph-Pery, TPE-Ph-Pery, and TPA-Ph-Pery CMPs. These CMPs were synthesized through effective Suzuki polymerizations of Py-Br_4, TPE-Br_4, and TPA-Br_3 with Pery-Br_2 and $PhB(OH)_2$ in the presence of K_2CO_3/Pd as the catalyst in solutions of DMF and H_2O, resulting in the formation of brown solid products. To assess the molecular characteristics and thermal degradation of the Py-Ph-Pery, TPE-Ph-Pery, and TPA-Ph-Pery CMPs, we conducted analyses using various techniques. The room-temperature FTIR spectra of the Pery-CMPs are depicted in Figure 2a, illustrating absorption signals related to the C−H aromatic, C═O anhydride, and C═C aromatic groups. The appearance absorption peaks of C═O groups for the redox-active Pery units in all Pery-CMPs indicate the successful incorporation of Pery units into the conjugated networks. ss ^{13}C NMR spectra (Figure 2b) proved the attainment of the Suzuki–Miyaura reaction, leading to the amplification of Py-Ph-Pery CMP, TPE-Ph-Pery CMP, and TPA-Ph-Pery CMP. The spectra exhibited signals corresponding to carbon nuclei in the Pery moiety, aromatic C═C, and the C═O groups in the Pery units. For the Py-Ph-Pery CMP, these signals were observed at 177.20 and 145.35−117.95 ppm, respectively. For the TPE-Ph-Pery CMP, the signals appeared at 178.00 and 147.05−117.56 ppm, and for the TPA-Ph-Pery CMP, the signals were observed at 176.94 and 149.95−118.90 ppm. The combined findings of the FTIR and ss ^{13}C NMR spectra were used to confirm the successful synthesis and presence of Pery redox units as structural ingredients in these three CMPs. For thermogravimetric analysis (TGA), we heated all three Pery-CMPs in a N_2 atmosphere to temperatures ranging from 40 to 800 °C (Figure 2c). Py-Ph-Pery, TPE-Ph-Pery, and TPA-Ph-Pery CMPs experienced 10% weight losses at temperatures of 498, 186, and 392 °C, respectively, under N_2 conditions. At 800 °C, the char yields of Py-Ph-Pery, TPE-Ph-Pery, and TPA-Ph-Pery CMPs were 80, 56, and 65 wt %, respectively. TGA demonstrated that our Pery-CMP materials exhibited enhanced thermal stability. Thus, these Pery-linked CMPs possess improved thermal stabilities, making them potentially valuable in various practical applications. Investigations using powder X-ray diffraction (PXRD) proved that all of the produced CMPs are in an amorphous state (Figure 2d).

To estimate S_{BET}, total pore volumes (V_{total}), and pore size diameters of Py-Ph-Pery, TPE-Ph-Pery, and TPA-Ph-Pery CMPs, we performed N_2 adsorption and desorption tests at

https://doi.org/10.1021/acsaem.3c01391
ACS Appl. Energy Mater. 2023, 6, 8277−8287

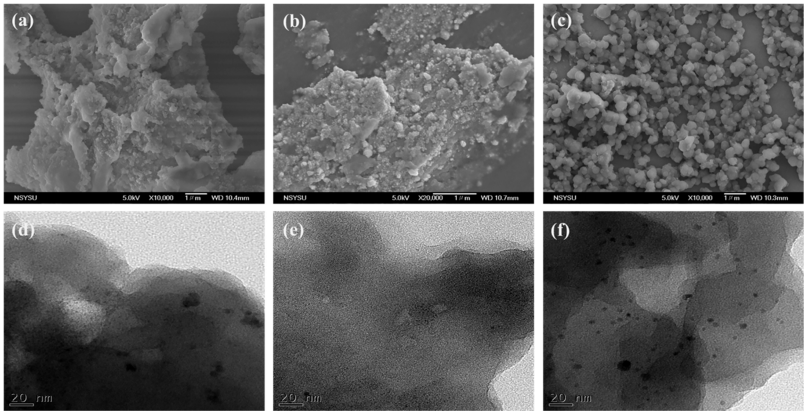

Figure 4. SEM and TEM images of Py-Ph-Pery (a, d), TPE-Ph-Pery (b, e), and TPA-Ph-Pery CMPs (c, f).

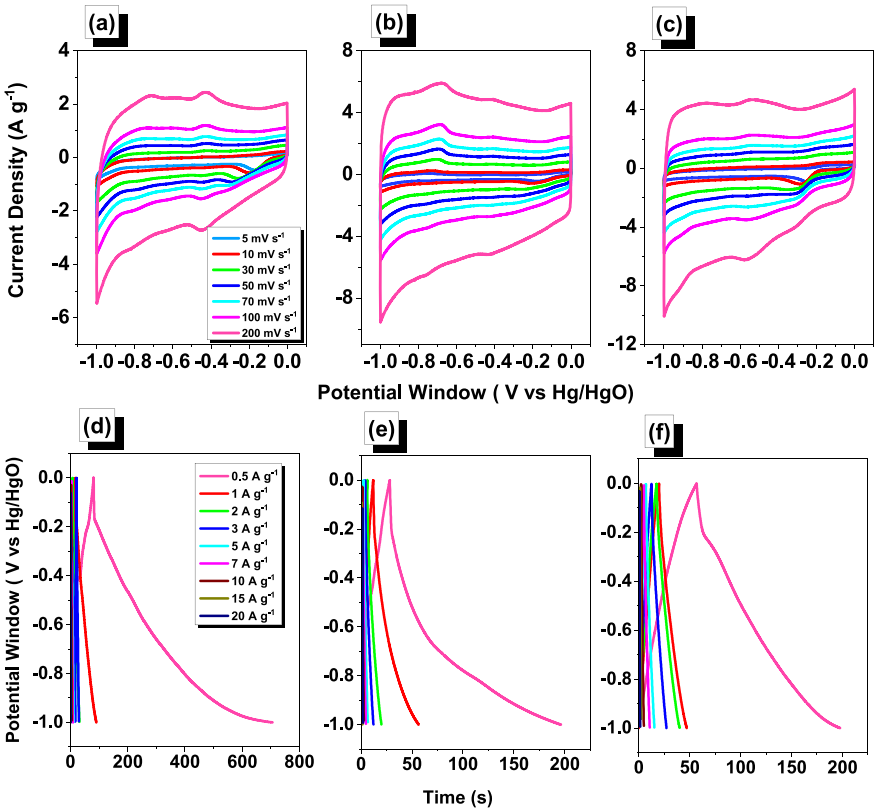

Figure 5. CV and GCD profiles of (a, d) Py-Ph-Pery, (b, e) TPE-Ph-Pery, and (c, f) TPA-Ph-Pery CMPs recorded in KOH (1 M).

77 K (Figure 3). Py-Ph-Pery, TPE-Ph-Pery, and TPA-Ph-Pery CMPs desorption processes all displayed detectable hysteresis, which suggested the presence of mesoporous framework structures. Additionally, according to the IUPAC classification, the N_2 isotherm profiles of the Py-Ph-Pery, TPE-Ph-Pery, and TPA-Ph-Pery CMPs showed type II and type IV curves, which suggested porous structures (Figure 3a–c).

The S_{BET} and V_{total} values for the Py-Ph-Pery CMP were 656 $m^2 g^{-1}$ and 0.09 $cm^3 g^{-1}$, respectively. For TPE-Ph-Pery CMPs, the corresponding values were 16 $m^2 g^{-1}$ and 0.05 $cm^3 g^{-1}$, while for the TPA-Ph-Pery CMP, the values were 12 $m^2 g^{-1}$ and 0.04 $cm^3 g^{-1}$. Moreover, the pore diameters of Py-Ph-Pery, TPE-Ph-Pery, and TPA-Ph-Pery CMPs are 1.78–2.3, 2.34, and 3.19 nm, respectively (Figure 3d–f). The difference in the Brunauer–Emmett–Teller (BET) surface area between the Py-Ph-Pery-CMP sample and the TPE-Ph-Pery CMP and TPA-Ph-Pery CMP samples may be owing to the Py molecule's molecular alignment during the procedure of polymers, which led to an elevated level of polymerization. The nanoscale size of these pores indicated the mesoporosity of the Pery-CMP frameworks.[65]

SEM and TEM analyses were employed to analyze the morphologies of the Py-Ph-Pery CMP, TPE-Ph-Pery CMP, and TPA-Ph-Pery CMP (Figure 4). SEM pictures [Figure 4a–c] revealed the presence of small aggregated spherical particles in all three Pery-CMPs. Additionally, the TEM photos [Figure 4d–f] showed bright and alternating clogged pores, indicating the porous structure of the Pery-CMPs.

Electrochemical Performance of Pery-CMPs in Three-Electrode and Symmetric Coin Cell Systems. The electrochemical performance of Pery-CMPs was evaluated using cyclic voltammetry (CV) and galvanostatic charge–

https://doi.org/10.1021/acsaem.3c01391
ACS Appl. Energy Mater. 2023, 6, 8277–8287

discharge (GCD) profiles in a 1.0 M KOH aqueous solution. Figure 5a–c exhibits the CV curves of the entire set of Pery-CMPs, encompassing a broad spectrum of scan speeds (ranging from 5 to 200 mV s^{-1}) and a potential range spanning from −1.0 to 0.0 V. The CV curves exhibited a distinctive quasi-rectangle-like humped shape, indicating reliable current sweeps and representing capacitance from EDLCs. The SC's storage capabilities are influenced by both redox and EDLC processes. In the CV curve of the Py-Ph-Pery CMP, two prominent redox peaks were observed—an oxidation peak at 0.42 V and a reduction peak at 0.45 V relative to Hg/HgO. This demonstrates the significance of redox processes in the material's behavior. In the CV curve of the TPE-Ph-Pery CMP, two prominent redox peaks or humps were observed—an oxidation peak at 0.67 and −0.41 V, a reduction peak at −0.75, and −0.43 V relative to Hg/HgO. In the CV curve of the TPA-Ph-Pery CMP, two prominent redox peaks or humps were observed—an oxidation peak at −0.54 V and a reduction peak at −0.56 V relative to Hg/HgO. This demonstrates the significance of redox processes in the material's behavior. This proves that the CV curves of both CMP exhibited a distinctive quasi-rectangle-like humped shape, indicating reliable current sweeps and representing capacitance from EDLC. When compared to TPE-Ph-Pery and TPA-Ph-Pery CMPs, Py-Ph-Pery CMP's wide surface and smaller pore dispersion are more significant due to their distinct differences in CV shape. This is because the total capacitance of the Py-Ph-Pery CMP is spread across the entire voltage range. The CV curves reveal that the specific capacitance falls when the scan rate rises as the oxidation–reduction process cannot fully react within shorter scan durations. Additionally, the compounds' capacitance and GCD curves were investigated at current densities from 0.5 to 20 A g^{-1} (Figure 5c–f). The GCD curves displayed a triangular shape with a slight bend, indicating both EDLC and pseudo-capacitive characteristics.[66−68] All compounds' discharge times were longer than their charging times, which suggest greater capacitance.[67] Higher capacitance was achieved at low scan rates because slower scan rates allow ions in the electrolyte sufficient time to reach and interact with all the active sites present in the charged materials. In contrast, faster scan rates facilitate more rapid access of the electrolyte to the electroactive components, resulting in a reduction in capacitance.[66−68]

When evaluated at a current density of 0.5 A g^{-1}, the Py-Ph-Pery CMP exhibited a specific capacitance of 300 F g^{-1}, while TPE-Ph-Pery and TPA-Ph-Pery CMPs displayed capacitances of 82 and 68 F g^{-1}, respectively (Figure 6a). Even with increasing current density, the Py-Ph-Pery CMP exhibited better specific capacitance compared to the TPE-Ph-Pery CMP and TPA-Ph-Pery CMP. The parent molecules' composition and dimension can be used to explain this propensity. The fused benzene rings in the Py subunit of the Py-Ph-Pery CMP facilitated strong contact and stable electron conductivity, creating pores for electrolyte ion transport.[69] Additionally, the larger surface area of the Py-Ph-Pery CMP contributed to its superior performance. As the current density increased, the specific capacitance of all three compounds gradually decreased. Charge storage occurred largely on the outside active surface because at higher current densities, ions in the electrolyte were unable to pass through the pores.[68] The long-term stability of these Pery-CMP compounds for electrochemical energy storage applications was demonstrated by their performance over 2000 charge/discharge cycles at 10 A g^{-1}, as shown in Figure 6b. The capacity retention over these cycles was determined to be 93% for the Py-Ph-Pery CMP,

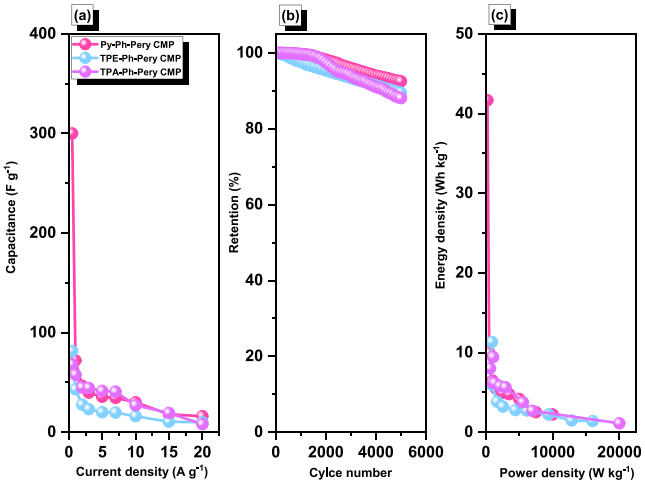

Figure 6. (a) Specific capacitance, (b) cycling stability profile, and (c) Ragone plot of Py-Ph-Pery, TPE-Ph-Pery, and TPA-Ph-Pery CMPs.

90% for the TPE-Ph-Pery CMP, and 88% for the TPA-Ph-Pery CMP. Based on the data, the Py-Ph-Pery CMP and TPA-Ph-Pery CMP exhibited better capacity retention and cycle durability among the three porous composites. This behavior can be attributed to the fused Py moieties in Py-Ph-Pery and the TPA-Ph-Pery CMP, which form strong $\pi-\pi$ stacking within the units, contributing to the stability and integrity of the materials over extended cycling periods. Furthermore, the energy density of the materials was determined based on the Ragone plot shown in Figure 6c. The energy density values for the Py-Ph-Pery CMP, TPE-Ph-Pery CMP, and TPA-Ph-Pery CMP were found to be 41.6, 11.3, and 9.44 Wh kg^{-1}, respectively. This indicates that the Py-Ph-Pery CMP exhibited the highest energy density, followed by the TPE-Ph-Pery CMP and TPA-Ph-Pery CMP. Table S1 presents the comparative performance analysis of our Pery-CMPs as organic electrodes in SC applications compared to other porous electrode materials.

Electrochemical impedance spectroscopy (EIS) was employed to examine the electrode–electrolyte interface within a specific frequency range in this study. A 1.0 M KOH aqueous solution was used as the electrolyte. The EIS curves were analyzed by fitting them with an equivalent circuit comprising several components, including R_s (equivalent series resistance), R_{ct} (charge transfer resistance), CPE-EDL (constant phase element representing electric double-layer capacitance), CPE-P (constant phase element representing pseudo-capacitance), and Z_w (Warburg element) (Figure 7a,b). The initial series resistance (Ohmic resistance) for TPA-Ph-Pery, TPE-Ph-Pery, and Py-Ph-Pery CMPs was determined to be 25.3, 26.1, and 11.2 Ω, respectively. Among the three compounds, the Py-Ph-Pery CMP exhibited the lowest resistance, indicating its favorable characteristics as an electrode material. Furthermore, the frequency-dependent magnitude Bode plot (Figure 7c) shows that all three porous materials exhibit outstanding capacitive performance when utilized as electrode compounds for energy-related applications. The frequency-dependent phase angle Bode plot (Figure 7d) revealed the knee frequencies, which are a sign of how quickly electrode materials work. The knee frequency is the frequency at which the capacitive and resistive features of the material are equal, and it serves as a measure of rate performance. Based on Figure 7d, the calculated knee frequencies for TPA-Ph-Pery, TPE-Ph-Pery, and Py-Ph-Pery CMPs were 360.99, 65.43, and 144.29 Hz, respectively. These

https://doi.org/10.1021/acsaem.3c01391
ACS Appl. Energy Mater. 2023, 6, 8277−8287

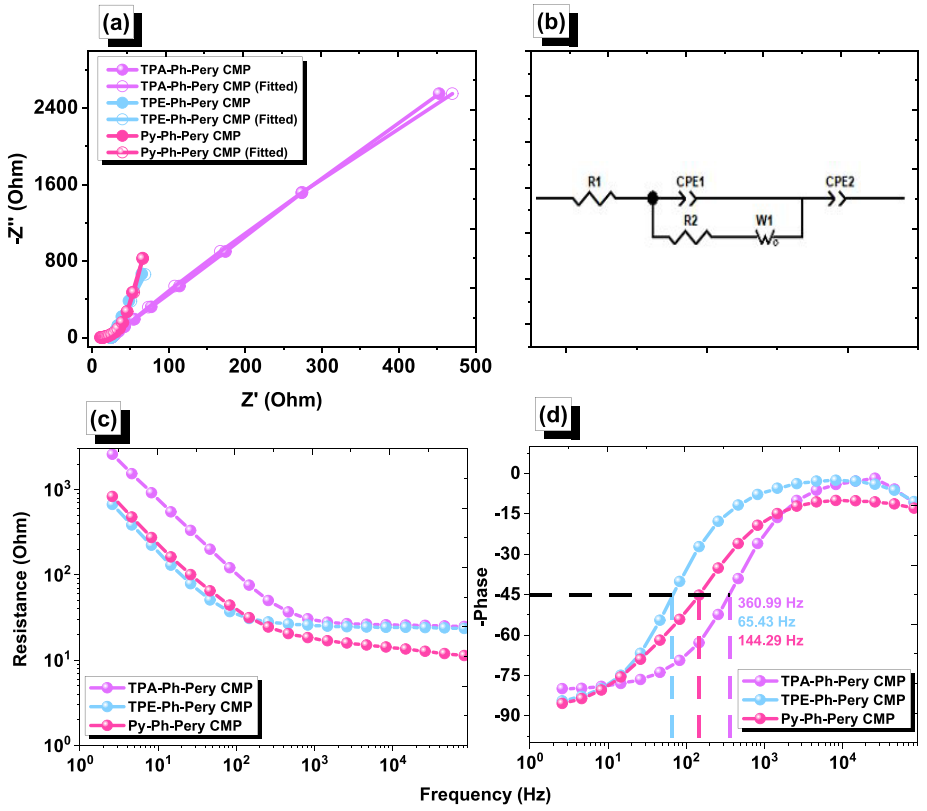

Figure 7. EIS curves: (a) Nyquist plots and (b) equivalent fitted circuit, (c) Bode plot of frequency-dependent resistance (magnitude), and (d) Bode plot of frequency-dependent phase angles of Py-Ph-Pery, TPE-Ph-Pery, and TPA-Ph-Pery CMPs.

findings show the materials' ability to use as electrodes in storing energy technologies.[70]

In our work, we utilized a CR2032 coin cell as the experimental setup, which consists of several components, including a bottom and top cover, metal spring, separator, anode, cathode, and electrolyte. The purpose was to investigate the electrochemical behavior of a symmetric SC (SSC). Specifically, we employed Pery-CMPs synthesized as both the cathode and anode materials of the symmetric SC. To prepare the CMP slurry, we followed the procedures outlined in our study and cast it onto carbon paper. The Selemion AMV membrane and a 1.0 M aqueous KOH electrolyte were used in our experiments. The electrochemical performance of the SSCs was assessed by performing CV measurements, covering a wide potential range of −0.6 to +0.6 V, while varying the scan speeds from 5 to 200 mV s^{-1}. The resulting CV curves (Figure 8a−c) of the Pery-CMPs exhibited characteristic rectangular shapes and crests in the lower potential region, indicative of SCs possessing both double-layer and pseudo-capacitive properties. Notably, the electrodes demonstrated favorable stability as the scan rate increased, signifying enhanced rate capability and material durability. Furthermore, we performed GCD measurements on the Py-Ph-Pery, TPE-Ph-Pery, and TPA-Ph-Pery CMPs electrodes, examining their performance at 1 to 10 A g^{-1} (Figure 8d−f). The GCD profiles exhibited nearly triangular shapes with minor curves, reflecting the synergistic impacts of pseudo-capacitance and EDLC.

At a current density of 1 A g^{-1}, the capacitances of the Py-Ph-Pery, TPE-Ph-Pery, and TPA-Ph-Pery CMPs were identified as 84, 26, and 23 F g^{-1}, respectively (Figure 9a). Notably, the Py-Ph-Pery CMP electrode demonstrated a higher capacitance compared to the other CMPs, likely due to its larger surface area facilitating improved ion mobility. To evaluate the cycling stability of the Pery-CMPs, we subjected them to 5000 charge−discharge cycles at 10 A g^{-1} (Figure 9b). The TPA-Ph-Pery CMP exhibited superior capacity retention (93.23%) compared to the Py-Ph-Pery CMP (87.85%) and TPE-Ph-Pery CMP (87.36%). This enhanced stability of the TPA-Ph-Pery CMP can be attributed to the presence of hetero atoms, which improve the interaction between the electrolyte and electrode, thereby contributing to higher capacity retention. The energy densities of the Py-Ph-Pery CMP, TPE-Ph-Pery CMP, and TPA-Ph-Pery CMP were found to be 23.33, 7.32, and 6.49 Wh kg^{-1}, respectively (Figure 9c). Overall, our study demonstrated the promising electrochemical performance of the synthesized CMPs as cathode and anode materials in SSCs. The CMPs exhibited desirable capacitance, rate capability, and cycling stability, making them potential candidates for energy storage applications.

CONCLUSIONS

We have successfully synthesized redox-active PDI-based CMPs using a simple Suzuki−Miyaura coupling process. These CMPs possess notable features such as extended π-conjugation (Py-Ph-Pery and TPE-Ph-Pery CMPs) and the inclusion of heteroatoms (TPA-Ph-Pery CMP). The impact of these characteristics on the performance of SC electrode materials has been investigated. The CMPs that were created had acceptable porosity, particular surface areas, and char yield. Electrochemical analysis reveals a combination of normal ELDC behavior and pseudo-capacitance tendencies, providing high capacitance values and outstanding cycling stability (over 2000 cycles). Among the CMPs studied, the Py-Ph-Pery CMP and TPE-Ph-Pery CMP demonstrate superior performance compared to the TPA-Ph-Pery CMP,

https://doi.org/10.1021/acsaem.3c01391
ACS Appl. Energy Mater. 2023, 6, 8277−8287

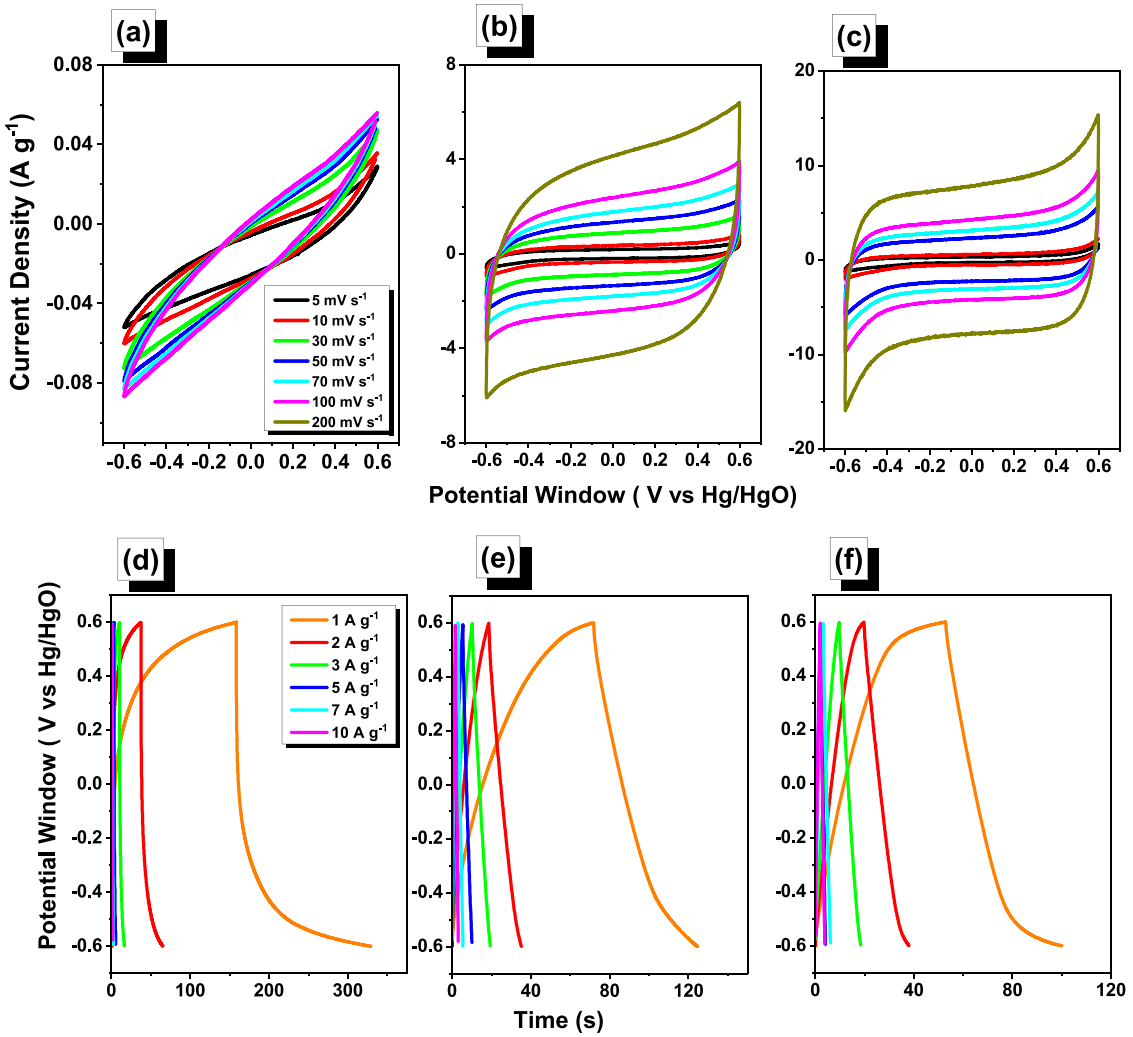

Figure 8. CV and GCD analyses of Py-Ph-Pery (a, c), TPE-Ph-Pery CMP (b, d), and TPA-Ph-Pery CMP (c, e) as organic electrodes for symmetric coin SCs.

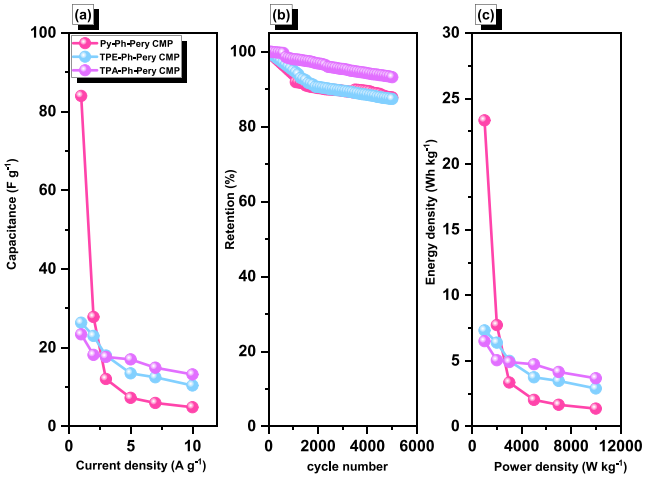

Figure 9. Cycle stability (a), durability (b), and Ragone (c) profiles of Py-Ph-Pery, TPE-Ph-Pery, and TPA-Ph-Pery CMPs as organic electrodes for SSCs.

primarily due to their continuous π-conjugation and their high surface area, respectively. Notably, the Py-Ph-Pery CMP exhibits the highest capacity of 300 F g^{-1}. These porous molecules exhibit outstanding results when utilized as symmetric coin cells in SCs, positioning them as promising electrode materials. Overall, the combination of facile synthesis, incorporation of redox-active groups, and favorable physical properties establishes these CMPs as effective cathode materials for SCs.

■ ASSOCIATED CONTENT

Supporting Information

The Supporting Information is available free of charge at https://pubs.acs.org/doi/10.1021/acsaem.3c01391.

Characterization and electrochemical analyses, schematic schemes of synthesized monomers in this study, FT-IR data of Pery-Br_2, and comparison of the specific capacitance of Pery-CMPs with those of previously reported materials for SC application (PDF)

■ AUTHOR INFORMATION

Corresponding Authors

Mohamed Gamal Mohamed − *Department of Materials and Optoelectronic Science, Center for Functional Polymers and Supramolecular Materials, National Sun Yat-Sen University, Kaohsiung 804, Taiwan; Department of Chemistry, Faculty of*

https://doi.org/10.1021/acsaem.3c01391
ACS Appl. Energy Mater. 2023, 6, 8277−8287

Science, Assiut University, Assiut 71515, Egypt; orcid.org/0000-0003-0301-8372; Email: mgamal.eldin12@yahoo.com

Shiao-Wei Kuo − *Department of Materials and Optoelectronic Science, Center for Functional Polymers and Supramolecular Materials, National Sun Yat-Sen University, Kaohsiung 804, Taiwan; Department of Medicinal and Applied Chemistry, Kaohsiung Medical University, Kaohsiung 807, Taiwan;* orcid.org/0000-0002-4306-7171; Email: kuosw@faculty.nsysu.edu.tw

Authors

Poonam Nagendra Singh − *Department of Materials and Optoelectronic Science, Center for Functional Polymers and Supramolecular Materials, National Sun Yat-Sen University, Kaohsiung 804, Taiwan*

Swetha V. Chaganti − *Department of Chemistry and International PhD Program for Science, National Sun Yat-Sen University, Kaohsiung 80424, Taiwan*

Santosh U. Sharma − *Department of Chemistry and International PhD Program for Science, National Sun Yat-Sen University, Kaohsiung 80424, Taiwan*

Moshin Ejaz − *Department of Materials and Optoelectronic Science, Center for Functional Polymers and Supramolecular Materials, National Sun Yat-Sen University, Kaohsiung 804, Taiwan*

Jyh-Tsung Lee − *Department of Chemistry and International PhD Program for Science, National Sun Yat-Sen University, Kaohsiung 80424, Taiwan; Department of Medicinal and Applied Chemistry, Kaohsiung Medical University, Kaohsiung 807, Taiwan;* orcid.org/0000-0002-2658-4222

Complete contact information is available at: https://pubs.acs.org/10.1021/acsaem.3c01391

Notes

The authors declare no competing financial interest.

■ ACKNOWLEDGMENTS

This study was supported financially by the Ministry of Science and Technology, Taiwan, under contracts NSTC 110-2124-M-002-013 and 111-2223-E-110-004. The authors thank the staff at National Sun Yat-Sen University for their assistance with the TEM (ID: EM022600) experiments.

■ REFERENCES

(1) Luo, Q.; Ma, H.; Hou, Q.; Li, Y.; Ren, J.; Dai, X.; Yao, Z.; Zhou, Y.; Xiang, L.; Du, H. All-carbon-electrode-based endurable flexible perovskite solar cells. *Adv. Funct. Mater.* **2018**, *28*, No. 1706777.

(2) Wei, Q.; Xiong, F.; Tan, S.; Huang, L.; Lan, E. H.; Dunn, B.; Mai, L. Porous one-dimensional nanomaterials: design, fabrication and applications in electrochemical energy storage. *Adv. Mater.* **2017**, *29*, No. 1602300.

(3) Mohamed, M. G.; Chang, W. C.; Kuo, S.-W. Crown Ether- and Benzoxazine-Linked Porous Organic Polymers Displaying Enhanced Metal Ion and CO_2 Capture through Solid-State Chemical Transformation. *Macromolecules* **2022**, *55*, 7879−7892.

(4) Ejaz, M.; Mohamed, M. G.; Kuo, S. W. Solid state chemical transformation provides a fully benzoxazine-linked porous organic polymer displaying enhanced CO_2 capture and supercapacitor performance. *Polym. Chem.* **2023**, *14*, 2494−2509.

(5) Mohamed, M. G.; Ahmed, M. M. M.; Du, W.-T.; Kuo, S.-W. Meso/Microporous Carbons from Conjugated Hyper-Crosslinked Polymers Based on Tetraphenylethene for High-Performance CO_2 Capture and Supercapacitor. *Molecules* **2021**, *26*, 738.

(6) Kundu, D.; Talaie, E.; Fau-Duffort, V.; Duffort, V.; Fau-Nazar, L. F.; Nazar, L. F. The emerging chemistry of sodium ion batteries for electrochemical energy storage. *Angew. Chem., Int. Ed.* **2015**, *54*, 3431−3448.

(7) Xiong, S.; Liu, J.; Wang, Y.; Wang, X.; Chu, J.; Zhang, R.; Gong, M.; Wu, B. Solvothermal synthesis of triphenylamine-based covalent organic framework nanofibers with excellent cycle stability for supercapacitor electrodes. *J. Appl. Polym. Sci.* **2022**, *139*, 51510.

(8) Zhao, X. Is Global Warming Mainly Due to Anthropogenic Greenhouse Gas Emissions? *Energy Sources, Part A* **2011**, *33*, 1985−1992.

(9) Mohamed, M. G.; Chang, S.-Y.; Ejaz, M.; Samy, M. M.; Mousa, A. O.; Kuo, S.-W. Design and Synthesis of Bisulfone-Linked Two-Dimensional Conjugated Microporous Polymers for CO_2 Adsorption and Energy Storage. *Molecules* **2023**, *28*, 3234.

(10) Samy, M. M.; Mohamed, M. G.; Kuo, S. W. Conjugated Microporous Polymers Based on Ferrocene Units as Highly Efficient Electrodes for Energy Storage. *Polymer* **2023**, *15*, 1095.

(11) Samy, M. M.; Mohamed, M. G.; Sharma, S. U.; Chaganti, S. V.; Mansoure, T. H.; Lee, J. T.; Tao Chen, T.; Kuo, S. W. Constructing conjugated microporous polymers containing triphenylamine moieties for high-performance capacitive energy storage. *Polymer* **2023**, *264*, No. 125541.

(12) Mohamed, M. G.; Hu, H. Y.; Madhu, M.; Samy, M. M.; Mekhemer, I. M. A.; Tseng, W. T.; Chou, H. H.; Kuo, S. W. Ultrastable two-dimensional fluorescent conjugated microporous polymers containing pyrene and fluorene units for metal ion sensing and energy storage. *Eur. Polym. J.* **2023**, *189*, No. 111980.

(13) Armand, M.; Tarascon, J. M. Building better batteries. *Nature* **2008**, *451*, 652−657.

(14) Young, C.; Park, T.; Yi, J. W.; Kim, J.; Hossain, M. S. A.; Kaneti, Y. V.; Yamauchi, Y. Advanced functional carbons and their hybrid nanoarchitectures towards supercapacitor applications. *ChemSusChem* **2018**, *11*, 3546−3558.

(15) Majumdar, D.; Baugh, N.; Bhattacharya, S. K. Ultrasound assisted formation of reduced graphene oxide-copper (II) oxide nanocomposite for energy storage applications. *Colloids Surf., A* **2017**, *512*, 158−170.

(16) Wang, F.; Li, G.; Zheng, J.; Ma, J.; Yang, C.; Wang, Q. Microwave synthesis of three-dimensional nickel cobalt sulfide nanosheets grown on nickel foam for high-performance asymmetric supercapacitors. *J. Colloid Interface Sci.* **2018**, *516*, 48−56.

(17) Mohamed, M. G.; Samy, M. M.; Mansoure, T. H.; Sharma, S. U.; Tsai, M. S.; Chen, J. H.; Lee, J. T.; Kuo, S. W. Dispersions of 1,3,4-Oxadiazole-Linked Conjugated Microporous Polymers with Carbon Nanotubes as a High-Performance Electrode for Supercapacitors. *ACS Appl. Energy Mater.* **2022**, *5*, 3677−3688.

(18) Mousa, A. O.; Zheng, I. L.; Chuang, C. H.; Chen, C. K.; Kuo, S. W.; Mohamed, M. G. Rational Design of Bifunctional Microporous Organic Polymers Containing Anthracene and Triphenylamine Units for Energy Storage and Biological Applications. *Int. J. Mol. Sci.* **2023**, *24*, 8966.

(19) Tan, J.; Han, Y.; He, L.; Dong, Y.; Xu, X.; Liu, D.; Yan, H.; Yu, Q.; Huang, C.; Mai, L. In situ nitrogen-doped mesoporous carbon nanofibers as flexible freestanding electrodes for high-performance supercapacitors. *J. Mater. Chem. A* **2017**, *5*, 23620−23627.

(20) Mousa, A. O.; Mohamed, M. G.; Chuang, C. H.; Kuo, S. W. Carbonized Aminal-Linked Porous Organic Polymers Containing Pyrene and Triazine Units for Gas Uptake and Energy Storage. *Polymers* **2023**, *15*, 1891.

(21) Sharma, S.; Soni, R.; Kurungot, S.; Asha, S. K. Naphthalene diimide copolymers by direct arylation polycondensation as highly stable supercapacitor electrode materials. *Macromolecules* **2018**, *51*, 954−965.

(22) Zhi, J.; Zhao, W.; Liu, X.; Chen, A.; Liu, Z.; Huang, F. Highly conductive ordered mesoporous carbon based electrodes decorated by 3D graphene and 1D silver nanowire for flexible supercapacitor. *Adv. Funct. Mater.* **2014**, *24*, 2013−2019.

(23) Simon, P.; Gogotsi, Y. Materials for electrochemical capacitors. *Nat. Mater.* **2008**, *7*, 845−854.
(24) Weber, J.; Thomas, A. Toward stable interfaces in conjugated polymers: microporous poly (p-phenylene) and poly (phenyleneethynylene) based on a spirobifluorene building block. *J. Am. Chem. Soc.* **2008**, *130*, 6334−6335.
(25) Thomas, A. Functional materials: from hard to soft porous frameworks. *Angew. Chem., Int. Ed.* **2010**, *49*, 8328−8344.
(26) Liao, Y.; Wang, H.; Zhu, M.; Thomas, A. Efficient supercapacitor energy storage using conjugated microporous polymer networks synthesized from Buchwald−Hartwig coupling. *Adv. Mater.* **2018**, *30*, No. 1705710.
(27) Cooper, A. I. Conjugated Microporous Polymers. *Adv. Mater.* **2009**, *21*, 1291−1295.
(28) Xu, Y.; Jin, S.; Xu, H.; Nagai, A.; Jiang, D. Conjugated microporous polymers: design, synthesis and application. *Chem. Soc. Rev.* **2013**, *42*, 8012−8031.
(29) Mohamed, M. G.; Tsai, M.-Y.; Wang, C.-F.; Huang, C.-F.; Danko, M.; Dai, L.; Chen, T.; Kuo, S.-W. Multifunctional Polyhedral Oligomeric Silsesquioxane (POSS) Based Hybrid Porous Materials for CO_2 Uptake and Iodine Adsorption. *Polymers* **2021**, *13*, 221.
(30) Samy, M. M.; Mekhemer, I. M. A.; Mohamed, M. G.; Elsayed, M. H.; Lin, K. H.; Chen, Y. K.; Wu, T. L.; Chou, H. H.; Kuo, S. W. Conjugated microporous polymers incorporating Thiazolo[5,4-d]-thiazole moieties for Sunlight-Driven hydrogen production from water. *Chem. Eng. J.* **2022**, *446*, No. 137158.
(31) Mohamed, M. G.; Sharma, S. U.; Liu, N. Y.; Mansoure, T. H.; Samy, M. M.; Chaganti, S. V.; Chang, Y. L.; Lee, J. T.; Kuo, S. W. Ultrastable Covalent Triazine Organic Framework Based on Anthracene Moiety as Platform for High-Performance Carbon Dioxide Adsorption and Supercapacitors. *Int. J. Mol. Sci.* **2022**, *23*, 3174.
(32) Luo, B.; Chen, Y.; Zhang, Y.; Huo, J. Nitrogen-rich anthraquinone−triazine conjugated microporous polymer networks as high-performance supercapacitor. *New J. Chem.* **2021**, *45*, 17278−17286.
(33) Amin, K.; Ashraf, N.; Mao, L.; Faul, C. F. J.; Wei, Z. Conjugated microporous polymers for energy storage: Recent progress and challenges. *Nano Energy* **2021**, *85*, No. 105958.
(34) Ejaz, M.; Samy, M. M.; Ye, Y.; Kuo, S.-W.; Mohamed, M. G. Design Hybrid Porous Organic/Inorganic Polymers Containing Polyhedral Oligomeric Silsesquioxane/Pyrene/Anthracene Moieties as a High-Performance Electrode for Supercapacitor. *Int. J. Mol. Sci.* **2023**, *24*, 2501.
(35) Weng, T.-H.; Mohamed, M. G.; Sharma, S. U.; Chaganti, S. V.; Samy, M. M.; Lee, J.-T.; Kuo, S.-W. Ultrastable Three-Dimensional Triptycene- and Tetraphenylethene-Conjugated Microporous Polymers for Energy Storage. *ACS Appl. Energy Mater.* **2022**, *5*, 14239−14249.
(36) Mohamed, M. G.; Atayde, E. C.; Matsagar, B. M.; Na, J.; Yamauchi, Y.; Wu, K. C. W.; Kuo, S.-W. Construction Hierarchically Mesoporous/Microporous Materials Based on Block Copolymer and Covalent Organic Framework. *J. Taiwan Inst. Chem. Eng.* **2020**, *112*, 180−192.
(37) Li, H.; Lyu, W.; Liao, Y. Engineering redox activity in conjugated microporous polytriphenylamine networks using pyridyl building blocks toward efficient supercapacitors. *Macromol. Rapid Commun.* **2019**, *40*, No. 1900455.
(38) Kou, Y.; Xu, Y.; Guo, Z.; Jiang, D. Supercapacitive energy storage and electric power supply using an aza-fused π-conjugated microporous framework. *Angew. Chem., Int. Ed.* **2011**, *50*, 8753−8757.
(39) Jiang, J. X.; Su, F.; Trewin, A.; Wood, C. D.; Campbell, N. L.; Niu, H.; Dickinson, C.; Ganin, A. Y.; Rosseinsky, M. J.; Khimyak, Y. Z.; Cooper, A. I. Conjugated microporous poly (aryleneethynylene) networks. *Angew. Chem., Int. Ed.* **2007**, *46*, 8574−8578.
(40) Jiang, J. X.; Wang, C.; Laybourn, A.; Hasell, T.; Clowes, R.; Khimyak, Y. Z.; Xiao, J.; Higgins, S. J.; Adams, D. J.; Cooper, A. I. Metal−organic conjugated microporous polymers. *Angew. Chem., Int. Ed.* **2011**, *50*, 1072−1075.
(41) Zhang, P.; Wu, K.; Guo, J.; Wang, C. From Hyperbranched Polymer to Nanoscale CMP (NCMP): Improved Microscopic Porosity, Enhanced Light Harvesting, and Enabled Solution Processing into White-Emitting Dye@NCMP Films. *ACS Macro Lett.* **2014**, *3*, 1139−1144.
(42) Ma, H.; Chen, J.-J.; Tan, L.; Bu, J.-H.; Zhu, Y.; Tan, B.; Zhang, C. Nitrogen-Rich Triptycene-Based Porous Polymer for Gas Storage and Iodine Enrichment. *ACS Macro Lett.* **2016**, *5*, 1039−1043.
(43) Chen, Q.; Luo, M.; Hammershøj, P.; Zhou, D.; Han, Y.; Laursen, B. W.; Yan, C.-G.; Han, B.-H. Microporous Polycarbazole with High Specific Surface Area for Gas Storage and Separation. *J. Am. Chem. Soc.* **2012**, *134*, 6084−6087.
(44) Chen, L.; Honsho, Y.; Seki, S.; Jiang, D. Light-Harvesting Conjugated Microporous Polymers: Rapid and Highly Efficient Flow of Light Energy with a Porous Polyphenylene Framework as Antenna. *J. Am. Chem. Soc.* **2010**, *132*, 6742−6748.
(45) Chen, L.; Yang, Y.; Jiang, D. CMPs as Scaffolds for Constructing Porous Catalytic Frameworks: A Built-in Heterogeneous Catalyst with High Activity and Selectivity Based on Nanoporous Metalloporphyrin Polymers. *J. Am. Chem. Soc.* **2010**, *132*, 9138−9143.
(46) Zhao, W.; Zhuang, X.; Wu, D.; Zhang, F.; Gehrig, D.; Laquai, F.; Feng, X. Boron-π-nitrogen-based conjugated porous polymers with multi-functions. *J. Mater. Chem. A* **2013**, *1*, 13878−13884.
(47) Liu, X.; Xu, Y.; Jiang, D. Conjugated Microporous Polymers as Molecular Sensing Devices: Microporous Architecture Enables Rapid Response and Enhances Sensitivity in Fluorescence-On and Fluorescence-Off Sensing. *J. Am. Chem. Soc.* **2012**, *134*, 8738−8741.
(48) Xu, Y.; Chen, L.; Guo, Z.; Nagai, A.; Jiang, D. Light-Emitting Conjugated Polymers with Microporous Network Architecture: Interweaving Scaffold Promotes Electronic Conjugation, Facilitates Exciton Migration, and Improves Luminescence. *J. Am. Chem. Soc.* **2011**, *133*, 17622−17625.
(49) Zhang, C.; Peng, L.-H.; Li, B.; Liu, Y.; Zhu, P.-C.; Wang, Z.; Zhan, D.-H.; Tan, B.; Yang, X.-L.; Xu, H.-B. Organic microporous polymer from a hexaphenylbenzene based triptycene monomer: synthesis and its gas storage properties. *Polym. Chem.* **2013**, *4*, 3663−3666.
(50) Zhao, Y.-C.; Wang, T.; Zhang, L.-M.; Cui, Y.; Han, B.-H. Microporous spiro-centered poly(benzimidazole) networks: preparation, characterization, and gas sorption properties. *Polym. Chem.* **2015**, *6*, 748−753.
(51) Zhang, Y.; A, S.; Zou, Y.; Luo, X.; Li, Z.; Xia, H.; Liu, X.; Mu, Y. Gas uptake, molecular sensing and organocatalytic performances of a multifunctional carbazole-based conjugated microporous polymer. *J. Mater. Chem. A* **2014**, *2*, 13422−13430.
(52) Gu, C.; Huang, N.; Chen, Y.; Qin, L.; Xu, H.; Zhang, S.; Li, F.; Ma, Y.; Jiang, D. π-conjugated microporous polymer films: designed synthesis, conducting properties, and photoenergy conversions. *Angew. Chem., Int. Ed.* **2015**, *54*, 13594−13598.
(53) Schmidt, J.; Werner, M.; Thomas, A. Conjugated microporous polymer networks via yamamoto polymerization. *Macromolecules* **2009**, *42*, 4426−4429.
(54) Dubey, P.; Bhardwaj, K.; Kumar, R.; Sundriyal, S.; Maheshwari, P. H. Perylene diimide incorporated activated carbon as a composite electrode for asymmetric supercapacitor. *J. Energy Storage* **2022**, *56*, No. 106058.
(55) Schon, T. B.; McAllister, B. T.; Li, P.-F.; Seferos, D. S. The rise of organic electrode materials for energy storage. *Chem. Soc. Rev.* **2016**, *45*, 6345−6404.
(56) Song, Z.; Zhou, H. Towards sustainable and versatile energy storage devices: an overview of organic electrode materials. *Energy Environ. Sci.* **2013**, *6*, 2280−2301.
(57) Liang, Y.; Yao, Y. Positioning organic electrode materials in the battery landscape. *Joule* **2018**, *2*, 1690−1706.
(58) Lin, Z.; Shi, H.-Y.; Lin, L.; Yang, X.; Wu, W.; Sun, X. A high capacity small molecule quinone cathode for rechargeable aqueous zinc-organic batteries. *Nat. Commun.* **2021**, *12*, 4424.
(59) Biradar, M. R.; Salkar, A. V.; Morajkar, P. P.; Bhosale, S. V.; Bhosale, S. V. Designing neurotransmitter dopamine-functionalized

naphthalene diimide molecular architectures for high-performance organic supercapacitor electrode materials. *New J. Chem.* **2021**, *45*, 9346−9357.
(60) Algharaibeh, Z.; Pickup, P. G. An asymmetric supercapacitor with anthraquinone and dihydroxybenzene modified carbon fabric electrodes. *Electrochem. Commun.* **2011**, *13*, 147−149.
(61) Biradar, M. R.; Kale, A. M.; Kim, B. C.; Bhosale, S. V.; Bhosale, S. V. Perylenediimide/Graphite Foil-Based Electrode Materials with Outstanding Cycling Stability for Symmetric Supercapacitor Device Architectures. *Energy Technol.* **2022**, *10*, No. 2200154.
(62) Seo, J.; Kantha, C.; Joung, J. F.; Park, S.; Jelinek, R.; Kim, J. M. Covalently linked perylene diimide−polydiacetylene nanofibers display enhanced stability and photocurrent with reversible FRET phenomenon. *Small* **2019**, *15*, No. 1901342.
(63) Li, R.; Xu, H.; Zhang, Y.; Chang, L.; Ma, Y.; Hou, Y.; Miao, S.; Wang, C. Electrochromic properties of pyrene conductive polymers modified by chemical polymerization. *RSC Adv.* **2021**, *11*, 39291−39305.
(64) Mohamed, M. G.; Elsayed, M. H.; Elewa, A. M.; EL-Mahdy, A. F. M.; Yang, C. H.; Mohammed, A. A. K.; Chou, H. H.; Kuo, S. W. Pyrene-containing conjugated organic microporous polymers for photocatalytic hydrogen evolution from water. *Catal. Sci. Technol.* **2021**, *11*, 2229−2241.
(65) Mohamed, M. G.; Sharma, S. U.; Yang, C.-H.; Samy, M. M.; Mohammed, A. A. K.; Chaganti, S. V.; Lee, J.-T.; Kuo, S. W. Anthraquinone-enriched conjugated microporous polymers as organic cathode materials for high-performance lithium-ion batteries. *ACS Appl. Energy Mater.* **2021**, *4*, 14628−14639.
(66) Mohamed, M. G.; Chaganti, S. V.; Sharma, S. U.; Samy, M. M.; Ejaz, M.; Lee, J.-T.; Zhang, K.; Kuo, S.-W. Constructing Conjugated Microporous Polymers Containing the Pyrene-4,5,9,10-Tetraone Unit for Energy Storage. *ACS Appl. Energy Mater.* **2022**, *5*, 10130−10140.
(67) Samy, M. M.; Mohamed, M. G.; Sharma, S. U.; Chaganti, S. V.; Lee, J.-T.; Kuo, S.-W. An Ultrastable Tetrabenzonaphthalene-Linked conjugated microporous polymer functioning as a high-performance electrode for supercapacitors. *J. Taiwan Inst. Chem. Eng.* **2023**, No. 104750.
(68) Samy, M. M.; Mohamed, M. G.; Kuo, S.-W. Pyrene-functionalized tetraphenylethylene polybenzoxazine for dispersing single-walled carbon nanotubes and energy storage. *Compos. Sci. Technol.* **2020**, *199*, No. 108360.
(69) Mohamed, M. G.; Chaganti, S. V.; Li, M.-S.; Samy, M. M.; Sharma, S. U.; Lee, J.-T.; Elsayed, M. H.; Chou, H.-H.; Kuo, S.-W. Ultrastable Porous Organic Polymers Containing Thianthrene and Pyrene Units as Organic Electrode Materials for Supercapacitors. *ACS Appl. Energy Mater.* **2022**, *5*, 6442−6452.
(70) Rafik, F.; Gualous, H.; Gallay, R.; Crausaz, A.; Berthon, A. Frequency, thermal and voltage supercapacitor characterization and modeling. *J. Power Sources* **2007**, *165*, 928−934.

https://doi.org/10.1021/acsaem.3c01391
ACS Appl. Energy Mater. 2023, 6, 8277−8287